Bulletin of the Mineral Research and Exploration

http://bulletin.mta.gov.tr

A contribution to the formation of the Karadut Iron Deposit (Kahramanmaraş-Göksun) and its surrounding mineralizations with new findings

Deniz TİRİNGA*[a], Nihat YILDIRIM[a], Ali DEMİR[a] and M. Remzi AYTAÇ[a]

[a]*Şimşek Group Construction and Mining Company, Çankaya/Ankara, Türkiye*

Research Article

Keywords:
Karadut, Synsedimentary, Hydrothermal, Kahramanmaraş, Magnetite, Hematite.

ABSTRACT

Karadut iron mineralization, situated between the Göksun and Elbistan districts in the Eastern Taurus. Many large and small iron deposits and mineralization are distributed across a 40-kilometer region south of the Sürgü fault. These mineralizations are notable not only for their high-grade ore but also for how they are formed. This study aims to investigate these mineralizations by analyzing their mineralogical characteristics and examining their spatial and temporal relationships with host rocks through field observations. Karadut iron mineralization comprises two primary types: metamorphic banded magnetite and hydrothermal hematite-goethite. Metamorphic banded mineralizations, observed as numerous deposits, offer small-scale reserves. Magnetites are aligned parallel to the lamination within micaschists, with thicknesses ranging from 1 cm to 10 m. Near-surface magnetites exhibit hematite formation via martitization, accompanied by supergene limonite formations. Analyses of outcrop and core samples reveal iron contents ranging from 34.20% to 85.14% Fe_2O_3. This study provides the first detailed exploration of hydrothermal-type mineralizations in high-altitude areas with limited accessibility. Mineralization developed along karstic voids and tectonic lines, primarily consisting of hematite and goethite, with barite as a gangue mineral. Outcrop samples indicate iron contents reaching 85.6% Fe_2O_3.

Received Date: 25.04.2025
Accepted Date: 01.08.2025

1. Introduction

The region between Göksun and Elbistan in Kahramanmaraş stands out for its extensive iron mineralizations, distributed across a significant area. This region is referred to as the "Ericek-Çardak (Berit Mountain) Iron Deposits" in the Iron Inventory of Türkiye, compiled by the General Directorate of Mineral Research and Exploration (Cihnioğlu et al., 1994). Initial investigations into the region's iron mineralizations were initiated by the General Directorate of Mineral Research and Exploration in the latter half of the 1970s and continued into the early 1990s. Atasever (1978) identified the iron ore as being compatible with the associated crystalline schists, sometimes manifesting as magnetite-bearing schist, and at other times as schist with magnetite, classifying it as sedimentary-metamorphic (itabirite). Bahçeci (1978) proposed that the mineralizations formed in a shallow marine environment proximal to land. Koç et al. (1985) noted that the iron ores occur at various levels within the schists, exhibit transitional characteristics with the host rock, and appear in lenticular and

Citation Info: Tiringa, D., Yıldırım, N., Demir, A. And Aytaç, M. R. 2025. A contribution to the formation of the Karadut iron deposit (Kahramanmaraş-Göksun) and its surrounding mineralizations with new findings. Bulletin of the Mineral Research and Exploration 178, 53-72. https://doi.org/10.19111/bulletinofmre.1768427

**Corresponding author: Deniz Tiringa, tiringadeniz@gmail.com*

wedge-like forms, indicative of sedimentary-type mineralization. They further observed that subsequent metamorphism, along with fracturing and folding processes, transformed these sedimentary formations into sedimentary-metamorphic deposits. Adıgüzel et al. (1991) highlighted that hematites within the Karadut iron mineralization were locally enriched and converted to magnetite due to metamorphic and tectonic activities. Hydrothermal-type mineralizations, characterized by hematite-goethite, have garnered attention due to increased production activities. This study provides a detailed evaluation of these hydrothermal mineralizations for the first time, alongside an assessment of magnetite mineralizations.

Iron ore production has significantly increased in the Karadut iron mineralization and neighboring deposits over the past decade, driven by rising demand. As a result, it has become essential to re-evaluate previous studies on the genesis of these mineralizations and to update existing findings by integrating recent data and insights. This approach aims to better inform exploration and production activities, by facilitating a deeper understanding of the mineralizations' characteristics. Improved efficiency in these activities is expected to make a more substantial contribution to the national economy.

1.1. Methods

Geochemical analyses were conducted on ore samples collected from drill cores and surface to determine their iron contents and other components. Drill core samples were systematically collected at intervals not exceeding one meter, with individual sampling carried out separately for each mineral species and ore texture. Surface sampling was performed at two-meter intervals, where a composite sample was obtained by mixing specimens collected from three distinct channels, each oriented perpendicular to the ore strike within the corresponding interval. These analyses were performed at the laboratories of the Department of Mineral Analysis and Technology (MAT) within the General Directorate of Mineral Research and Exploration (MTA). Major oxide compositions were analyzed using X-ray fluorescence (XRF) technology.

Mineralogical and petrographic studies were carried out at the Mineralogical-Petrographic Laboratories of the Mineral Analysis and Technology Department of the General Directorate of Mineral Research and Exploration. Thin and polished sections of the samples were prepared as a preliminary step. The thin sections were analyzed using a Leitz polarizing microscope to examine the rocks' mineralogical, petrographic, and textural properties. Ore microscopy studies on the polished sections were conducted using a Leica reflected-light microscope.

2. Geology

The study area is situated in the Eastern Taurus Mountains, within Karadut Village, Göksun District of Kahramanmaraş Province (Figure 1). The region exhibits metamorphic and structural units with diverse lithologies, dating from the Late Devonian to Late Cretaceous. The geological sequence is underlain by the Cretaceous Kömürhan (Göksun/İspendere) Ophiolite Nappe, which is tectonically overlain by the Late Devonian–Late Cretaceous Bodrum nappe (Malatya/Binboğa metamorphics). Lithologies of the Kömürhan Ophiolite and Bodrum Nappe are intruded by the Early-Middle Eocene Havcılar Granite (Perinçek and Kozlu, 1984*a*; Tarhan, 1984; Baydar, 1989; Pehlivan et al., 1991; Yılmaz et al., 1997; Bedi et al., 2005; Parlak, 2006; Bedi et al., 2017*a, b*; Kıral and Bedi, 2019). The entire sequence is unconformably overlain by Quaternary slope debris (Figure 2).

The Kömürhan Ophiolite is located at the base of the study area. The outcrops in the study area were initially referred to by this name by Bedi et al. (2004, 2005, 2009, 2012, 2017*a, b*) and Bedi and Yusufoğlu (2018) to ensure consistency in nomenclature across the Eastern Taurides. Outcrops are also observed on the southern slopes of Berit Mountain, near Taşlık Hill, south of the study area. Dominant lithologies include dark green to green serpentinites, lherzolites and harzburgites from peridotites, and banded gabbros, which often display intense cataclastic deformation and localized mylonitization (Figure 3). Epidotization is prominently evident. In the Taşlık Hill outcrops, lherzolites feature magnetite veinlets, while serpentinites contain minor disseminated chromite (Figure 4). Göncüoğlu and Turhan (1985) stated

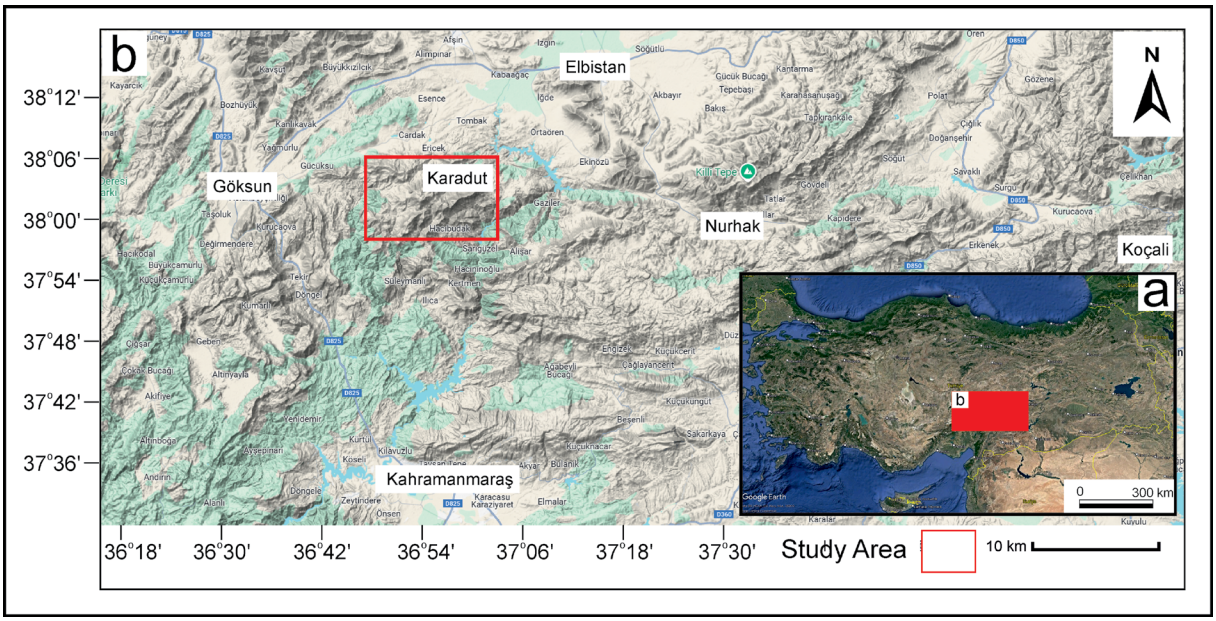

Figure 1- Location map of the study area.

that the ophiolitic rocks in the region are remnants of the southern branch of the Neotethys Ocean, while Robertson et al. (2012, 2013) and Karaoğlan et al. (2013) suggested that they were formed in the Berit Ocean, which developed between the Bitlis–Pütürge metamorphic units and the Tauride platform. Robertson et al. (2012), Parlak et al. (2013), and Nurlu et al. (2014) reported the presence of two parallel ophiolite belts trending NE–SW across Southeastern Anatolia. One of these belts is situated between the Keban–Malatya metamorphic units, which belong to the Tauride platform, and the Bitlis–Pütürge massifs, and it includes the Göksun–Berit (Kahramanmaraş), Meydan (Kahramanmaraş), Ispendere (Malatya), Killan (Diyarbakır), and Kömürhan–Guleman (Elazığ) Ophiolites. The ophiolitic slices accreted to the Tauride platform have been reported to be of Late Cretaceous age and of the supra-subduction zone (SSZ) type (Parlak et al., 2009). Tarhan (1982) proposed that these ophiolites formed in an oceanic environment during the Jurassic–Early Cretaceous, while Bedi et al. (2017*a*, *b*) suggested their emplacement predates the Campanian. Radiometric dating of the Ispendere and Kömürhan Ophiolites has yielded ages ranging from 84 to 88 Ma (Parlak et al., 2010; Karaoğlan, 2012).

The metamorphic units in the region, identified as the Bodrum nappe, have been referred to by various names in earlier studies, such as Keban metamorphics (Perinçek, 1979; Perinçek and Kozlu, 1984*a, b*), Keban and Malatya Nappes (Yazgan, 1981, 1984), Kabaktepe and Çağılhan metamorphics (Tarhan, 1982, 1984), Göksun metamorphics (Metin et al., 1982, 1986), Engizek unit (Baydar, 1989), Malatya metamorphics (Perinçek and Kozlu, 1984*a, b*; Yiğitbaş, 1989; Yıldırım, 1989; Karaman et al., 1993), and Binboğa metamorphics (Yılmaz et al., 1987*a, b*; Şenel et al., 2002; Bedi et al., 2005). Bedi et al. (2004, 2005, 2009, 2012, 2016, 2017*a, b*) and Bedi and Yusufoğlu (2018) have standardized these units as classifications under the Bodrum Nappe, due to their similarities to the Bodrum nappe observed in the Western-Central Taurides.

At the base of the Bodrum Nappe lies the Yoncayolu Formation, dated to the Late Devonian–Carboniferous period. Key structural elements include large overturned or recumbent folds and smaller-scale microfolds. The basal section is represented by the Büyükkızılcık Member, characterized by intensely folded yellow-brown, white, and green quartzites, quartz schists, graphite schists of varying compositions, and bituminous metashales. These are interspersed with recrystallized limestone, marble, dolomite, dolomitic limestone, and calc-schist layers. The overlying Apıklar Member is conformably

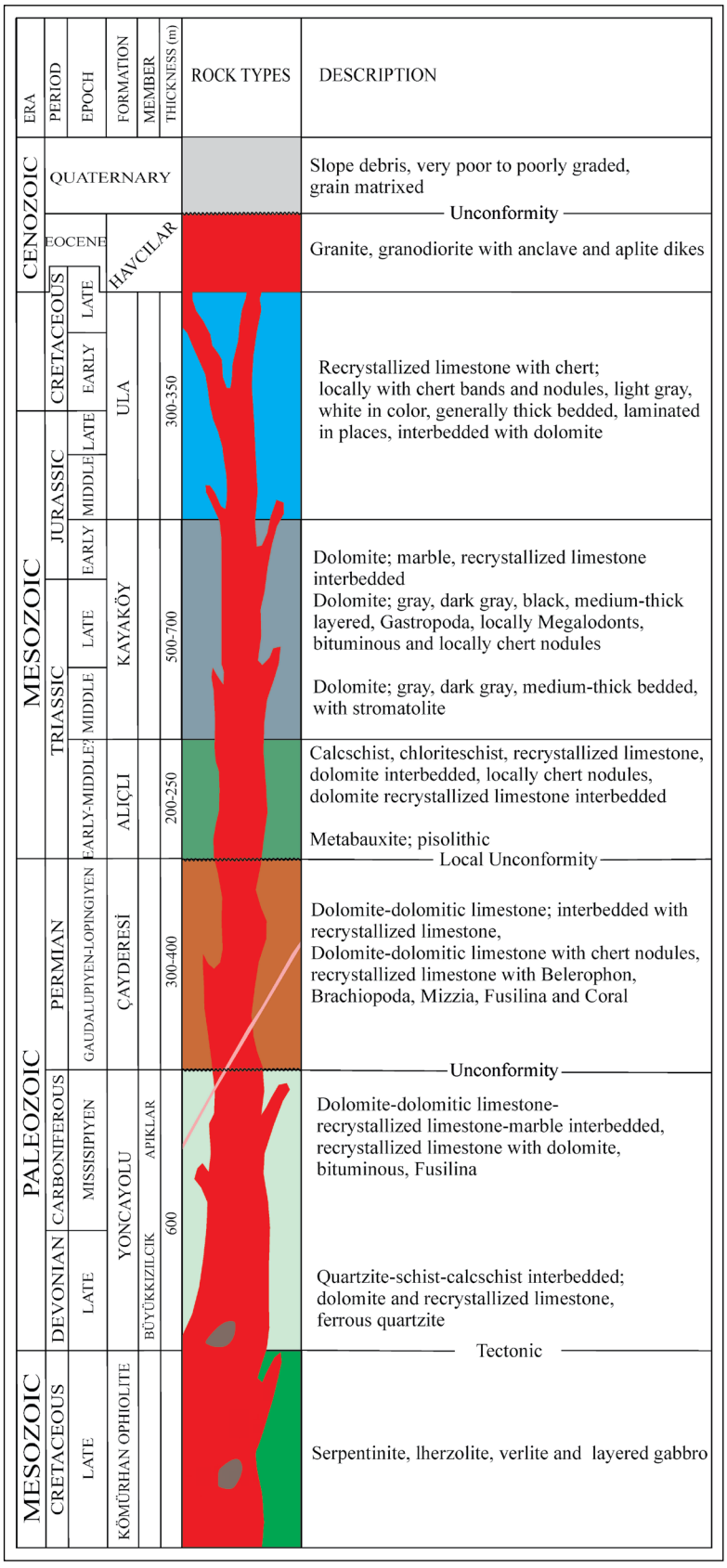

Figure 2- Generalized stratigraphic column section of the study area (modified from Kıral and Bedi, 2019).

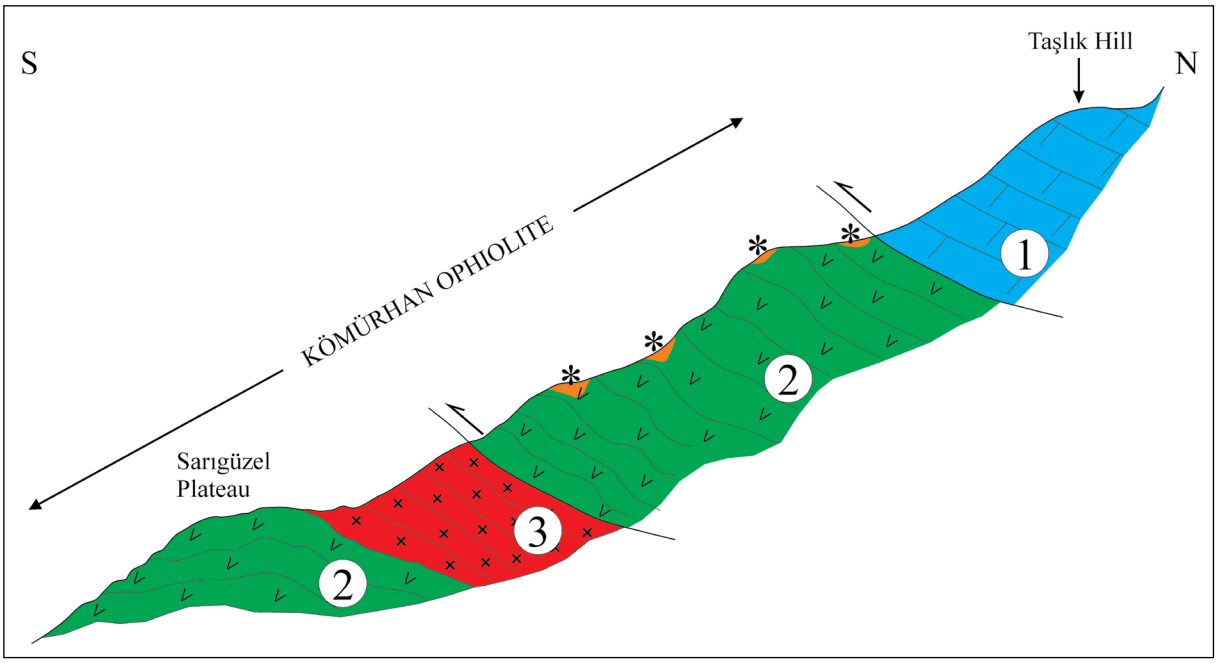

Figure 3- The cross section of the Kömürhan Ophiolite at the Taşlık Hill site (not to scale). (1. recrystallized limestones belonging to the Ula Formation, 2. greenish-brown colored, laminated and thinly bedded peridotites with folded and fractured, predominantly composed of amphibole and pyroxene, containing disseminated and vein-type magnetite locally abundant, and 3. dark green to whitish-colored, fine- to medium-grained banded gabbros, mainly composed of pyroxene and quartz, with locally abundant magnetite (The peridotites exhibit superficial hematite-limonite alteration).

Figure 4- a) outcrop view of cataclastic serpentinites, b) lherzolites containing magnetite veinlets (some veinlets have been interpreted and highlighted on the image).

composed of gray to dark gray dolomitic limestone, dolomite, and recrystallized limestone, occasionally intercalated with schist and metashale layers (Kıral and Bedi, 2019). This sequence exhibits moderate-grade metamorphism within the amphibolite facies (Yılmaz et al., 1997) (Figure 5).

The Middle–Late Permian Çayderesi Formation, which lies unconformably at the base, consists of alternating gray–dark gray and white dolomite, dolomitic limestone, recrystallized limestone, and marble, with minor intercalations of schist and calc-schist (Kıral and Bedi, 2019). This unit exhibits metamorphism characteristic of the low-grade amphibolite or greenschist facies (Yılmaz et al., 1997). Above it, with a local unconformity, lies the Early–Middle Triassic Alıçlı formation. At its base, this Formation contains occasional metabauxite levels and predominantly features alternations of green chlorite-quartz schist and calc-schist. Interlayers of cherty marble, recrystallized limestone, dolomite, and dolomitic limestone are occasionally observed within the formation (Kıral and Bedi, 2019). Low-grade metamorphism within the greenschist facies characterizes this unit (Yılmaz et al., 1997). Conformably overlying the Alıçlı Formation is the Middle–Late Triassic–Late Cretaceous Kayaköy Formation. This formation begins with medium to thick-bedded stromatolitic limestones at its base, transitioning upward into dark gray, massive dolomites. Occasional interlayers of white to light gray recrystallized limestone are present within the dolomites (Kıral and Bedi, 2019). Laterally transitional to the Kayaköy Formation, the Dogger–Late Cretaceous Ula formation comprises alternating recrystallized limestone, marble, calc-schist, and dolomite, with brecciated limestone at its upper levels (Kıral and Bedi, 2019). The recrystallized limestones, light gray to white in color, are generally massive, featuring dissolution cavities and saccharoidal textures (Figure 6).

The Havcılar Granite, which intrudes the Kömürhan Ophiolite and the Bodrum Nappe, is composed of gray and pinkish granite. It commonly displays a jointed structure and granoblastic texture, mainly consisting of quartz, oligoclase, orthoclase, and mica, with minor amounts of epidote and zircon (Yılmaz et al., 1997). Additionally, it contains enclaves of mafic and intermediate rocks such as gabbro and is intruded by aplite and mafic lamprophyre dykes (Tarhan, 1984; Kıral and Bedi, 2019). The age of the Havcılar Granite has been variously interpreted: Yılmaz et al. (1997) suggested a Late Paleozoic age, Tarhan (1982) proposed a Late Cretaceous age, and Kıral and Bedi (2019) determined an Early Eocene age based on K/Ar dating of biotite minerals.

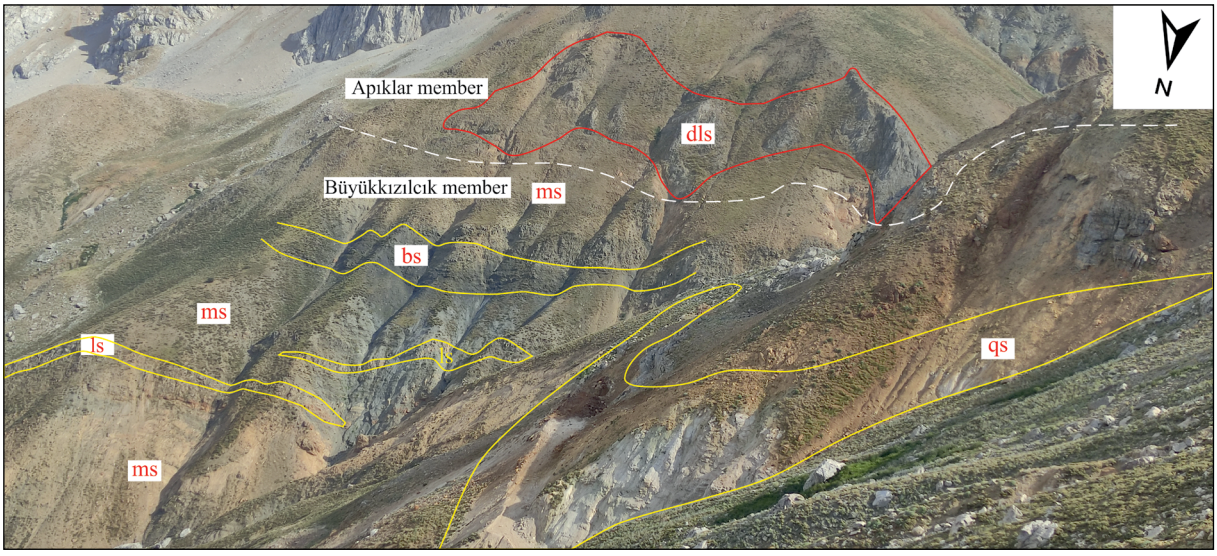

Figure 5- Field view of the lithologies of the Yoncayolu Formation. The white dashed line indicates inferred (approximate) contact of the Büyükkızılcık and Apıklar Members (ms: mica schist, bs: bituminous schist, qs: quartz schist, ls: limestone, dls: dolomitic limestone).

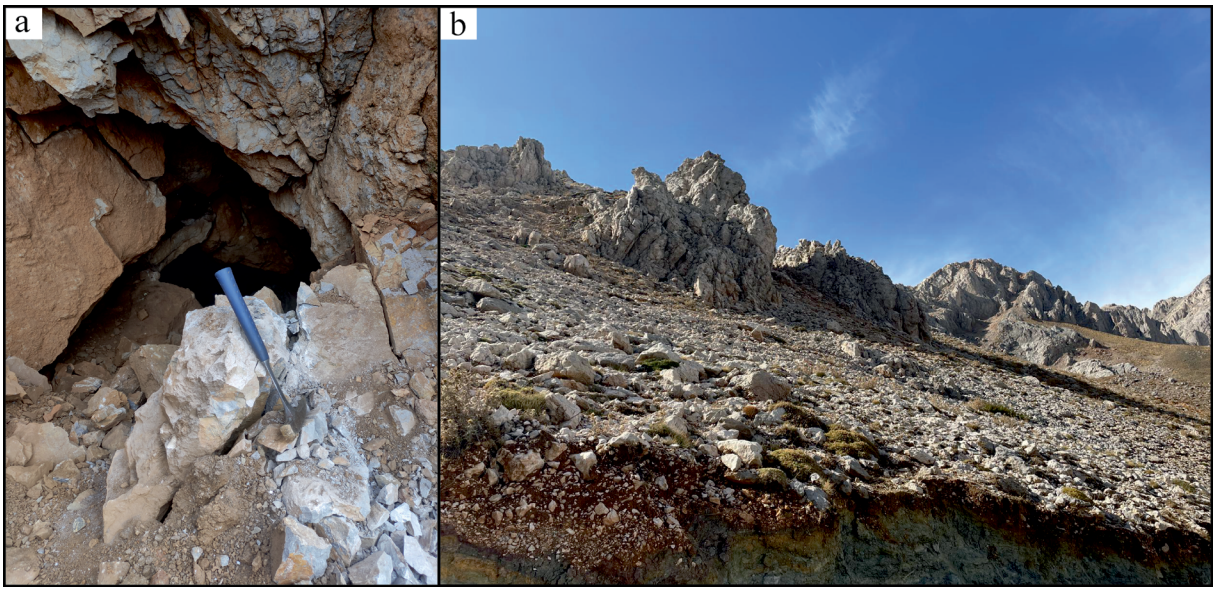

Figure 6- The field view of the limestones of the Ula formation in the field, a) limestone with dissolution cavities, b) recrystallized limestones.

The study area's steep-sloped topography is dominated by extensive slope debris, which unconformably covers the underlying units. These debris deposits consist of poorly to very poorly graded, grain-matrixed, semi-consolidated, generally angular pebbles that can reach block sizes. Their thickness varies depending on the slope gradient.

3. Results

Field observations in the study area have revealed the geological position, textural-structural relationships, and types of mineralization present. Comprehensive mineralogical and geochemical analyses of collected samples were conducted to interpret the formation processes of these mineralizations and evaluate their economic potential.

3.1. Field Observations

Field observations in the study area have identified two distinct types of iron mineralization: (i) magnetite mineralization and (ii) hematite-goethite mineralization. These two types differ in their formation processes, mineral paragenesis, modes of occurrence, and ages. Additionally, previous studies in the region have documented the presence of other metallic mineralizations, including chromium, copper, lead-zinc, as well as natural dimension stones (Kraeff, 1964; Bulur, 1969; Polat, 1970; Çalgın and Şişman, 1974; Zaralıoğlu and İnan, 1982; Vergili et al., 2017).

(i) Magnetite mineralization is observed within the upper levels of crystalline schists with varied compositions, such as green-colored amphibolite schist, mica schist, chlorite schist, and quartz schist, which are part of the Büyükkızılcık Member of the Devonian Yoncayolu Formation. This mineralization exhibits a wide distribution, extending over kilometers with continuity (Figure 7). Although interruptions in continuity occur due to fracturing, fragmentation, folding, erosion, and burial, the mineralization reappears at various locations. The mineral paragenesis primarily consists of magnetite, accompanied by hematite, pyrite, chalcopyrite, goethite, and limonite. Silica and carbonate are observed as gangue minerals (Figure 8).

Field observations have identified magnetite occurrences in two distinct forms: (1) massive and (2) disseminated. (1) Massive magnetites conform to the schistosity of the host rocks, with thicknesses ranging from a few millimeters to up to ten meters. These magnetites exhibit pervasive folding and prominent schistosity features consistent with the surrounding rock. Pyrite is frequently observed in association with massive magnetites, either aligned alongside the magnetite or forming clusters. Martitized zones within

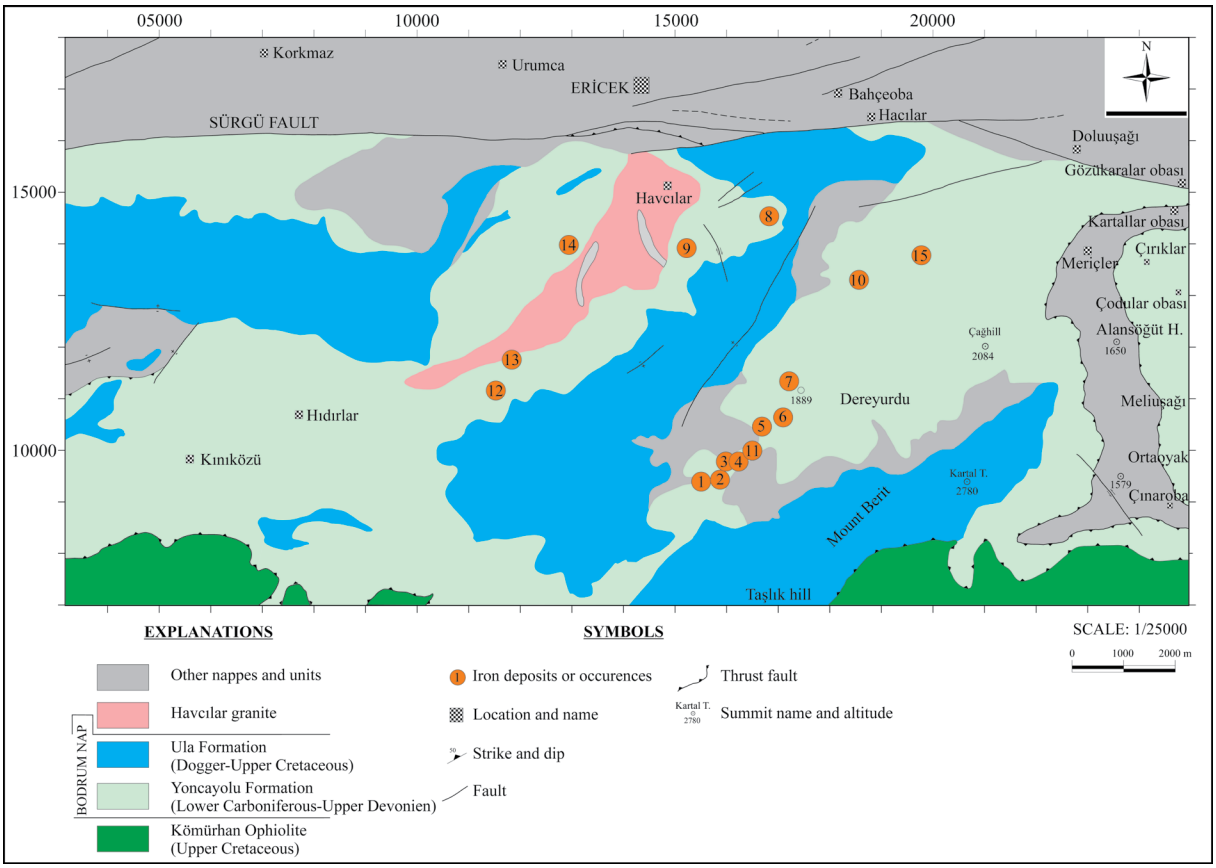

Figure 7- Geology map of iron deposits and occurrences in study area and surroundings (modified from Adıgüzel et al., 1991).

the magnetites maintain schistosity characteristics similar to the host rocks. Near-surface martitized ores have undergone alteration to goethite, with supergene enrichment processes leading to limonitization. (2) Disseminated magnetites are distributed within the host rocks and observed in varying grain sizes. These occurrences are occasionally concentrated in localized zones (Figure 9).

(ii) The goethite-hematite mineralization in the region is documented comprehensively for the first time in this study. It is observed within fractures, cracks, and karstic cavities of dissolution-prone recrystallized limestones belonging to the Middle Triassic–Late Cretaceous Ula Formation, where it partially or completely fills these cavities, exhibiting an irregular geometry. The mineral paragenesis primarily consists of goethite, accompanied by lesser amounts of hematite, limonite, and ankerite, with barite present as a gangue mineral. Along specific tectonic lines within the limestones, malachite and azurite have also been identified in association with hematites (Figure 10).

The mineralization within karstic cavities shows a gradient in quality, with higher grades near the central zones of the fillings. In these centers, goethite ores display colloform, kidney-like, and botryoidal textures, whereas in the outer zones, they appear as stains and replacements. Additionally, the mineralization is observed in brecciated forms within fracture and fault zones, where it acts as a cement for angular fragments of the wall rock. Based on textural and structural analyses, it is evident that hydrothermal processes played a significant role in the emplacement of this mineralization.

3.2. Ore Mineralogy

Microscopic analyses were performed on various ore samples to identify the constituent ore minerals, examine their textural properties, and gather insights into their formation processes. The ore minerals

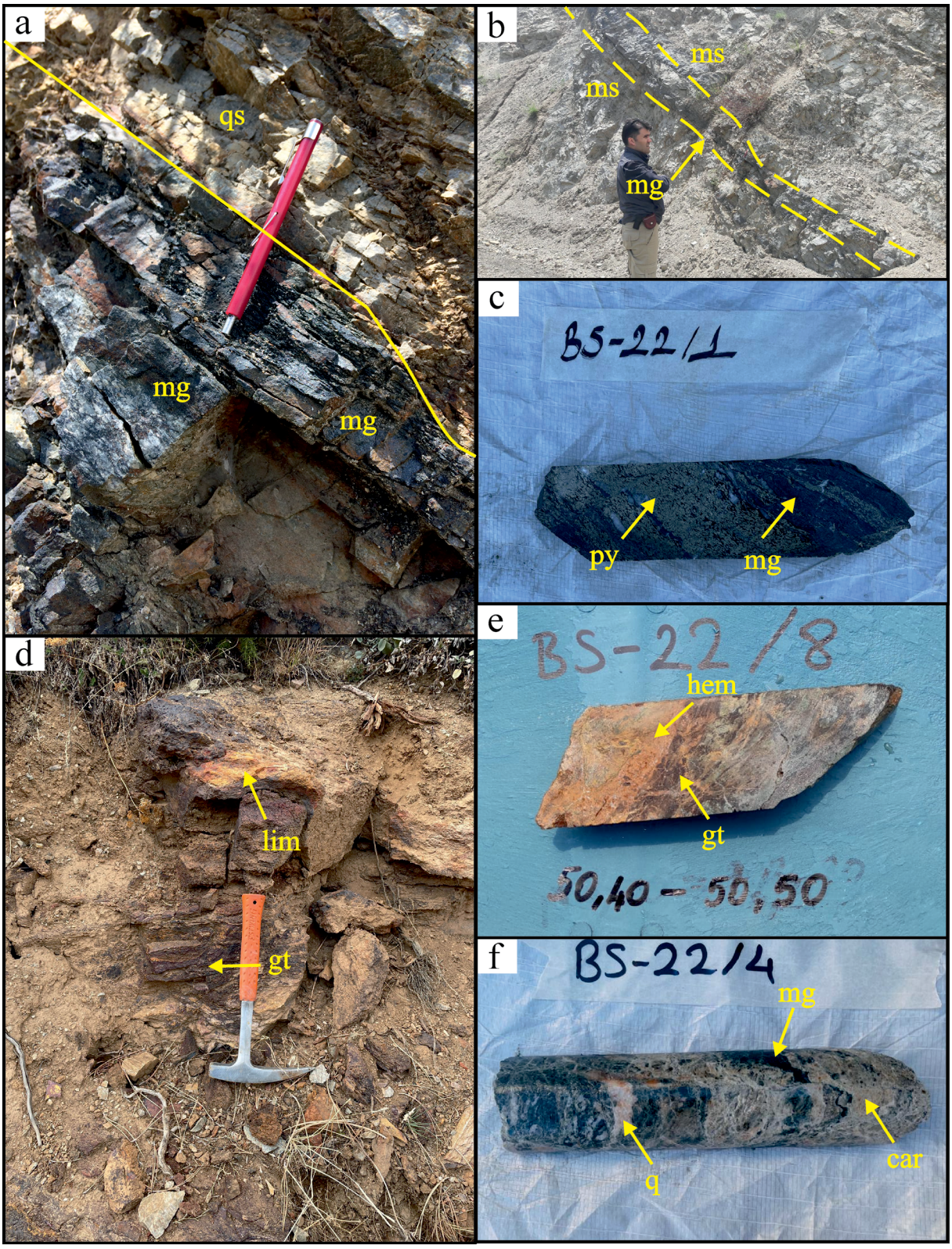

Figure 8- a) field image of magnetites lens parallel to quartzschists, b) field image of magnetite lens within micaschists, c) drill core image of pyrites parallel to orientation within magnetites, d) field image of magnetites converted to goethite and limonitization, e) drill core image of hematite and goethite transformations resulting from martitization in magnetites, f) drill core image of carbonate and quartz observed as gangue minerals in magnetites (mg: magnetite, qs: quartzschists, ms: micaschist, hem: hematite gt: goethite, py: pyrite, q: quartz, car: carbonate).

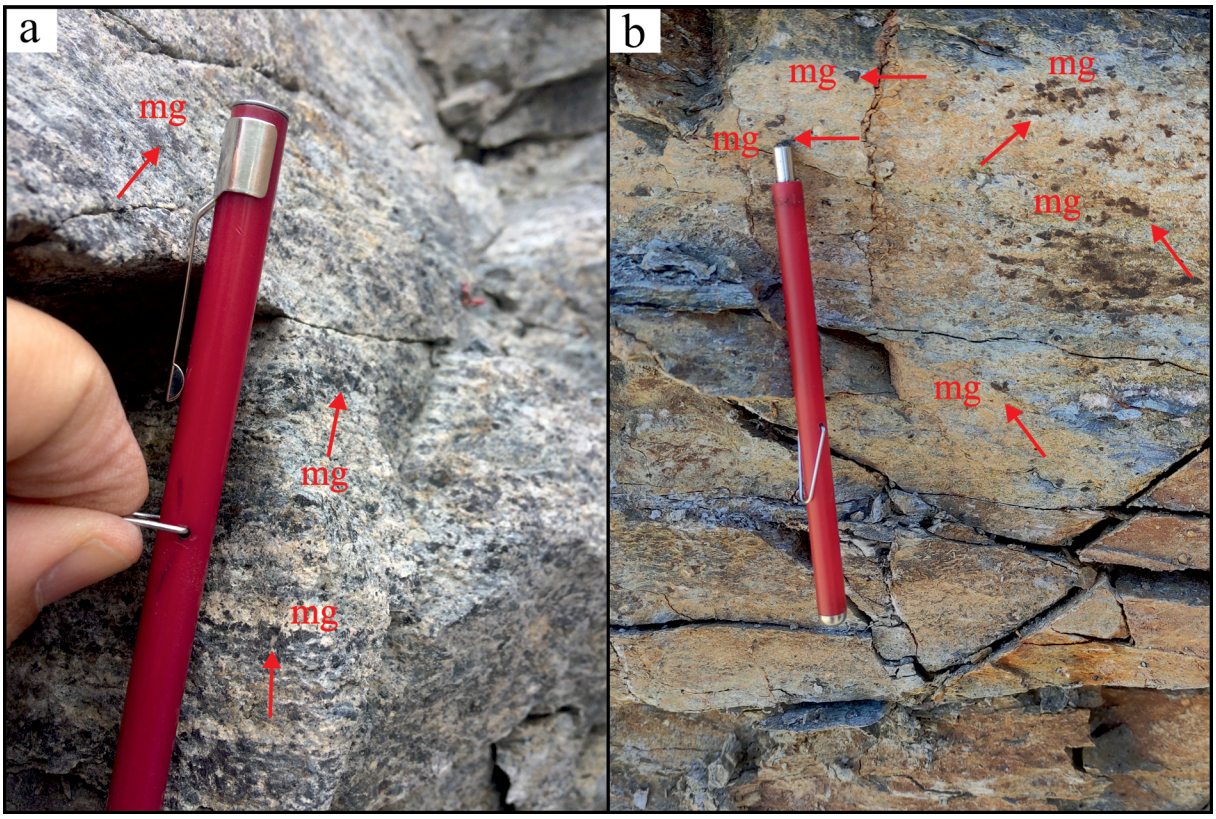

Figure 9- Field images of disseminated magnetite mineralization: a) densely disseminated magnetites parallel to micaschists, b) disseminated magnetites, occasionally coarse-grained, within quartzschists (mg: magnetite).

observed under the microscope include magnetite, pyrite, hematite, goethite, limonite, and chalcopyrite.

(i) Magnetite grains occur in both euhedral and anhedral forms, with sizes ranging from 0.08 mm to 4.5 mm. They are generally aligned parallel to the foliation and frequently host hematite inclusions within fractures, cracks, and cleavage planes, as well as occasionally within the magnetite grains themselves. Hematite grain sizes range from 0.05 mm to 4 mm. Evidence of martitization is observed in some sections, indicating the transformation of magnetite into hematite. Additionally, small pyrite and chalcopyrite grains are present within certain magnetites. Pyrites are anhedral, with the largest measured grain size reaching 900 microns. In some instances, pyrites crosscut magnetite grains, suggesting their formation postdating magnetite mineralization (Figure 11). Chalcopyrites, occurring in trace amounts, are also anhedral, present as small grains within pyrites. Occasionally, chalcopyrites display evidence of digenite transformation along their edges.

(ii) Goethite minerals are identified under the microscope in two distinct forms: massive and stockwork veinlets. Stockwork veinlet goethites exhibit iron oxide coloring, accompanied by submicroscopic goethite and occasional hematite inclusions. Within the goethite samples, very small remnants of pyrites, measuring less than 0.02 mm, are also observed. The presence of remnant pyrites and hematites within the goethite suggests that the mineralization originated from these precursor minerals (Figure 12).

3.3. Geochemical Analysis

During the field studies, 101 ore samples representing various mineralization types -including 39 massive and 25 disseminated magnetite, 7 martitized hematite, and 30 hydrothermal goethite- were collected from surface outcrops and drill cores and subsequently analyzed geochemically.

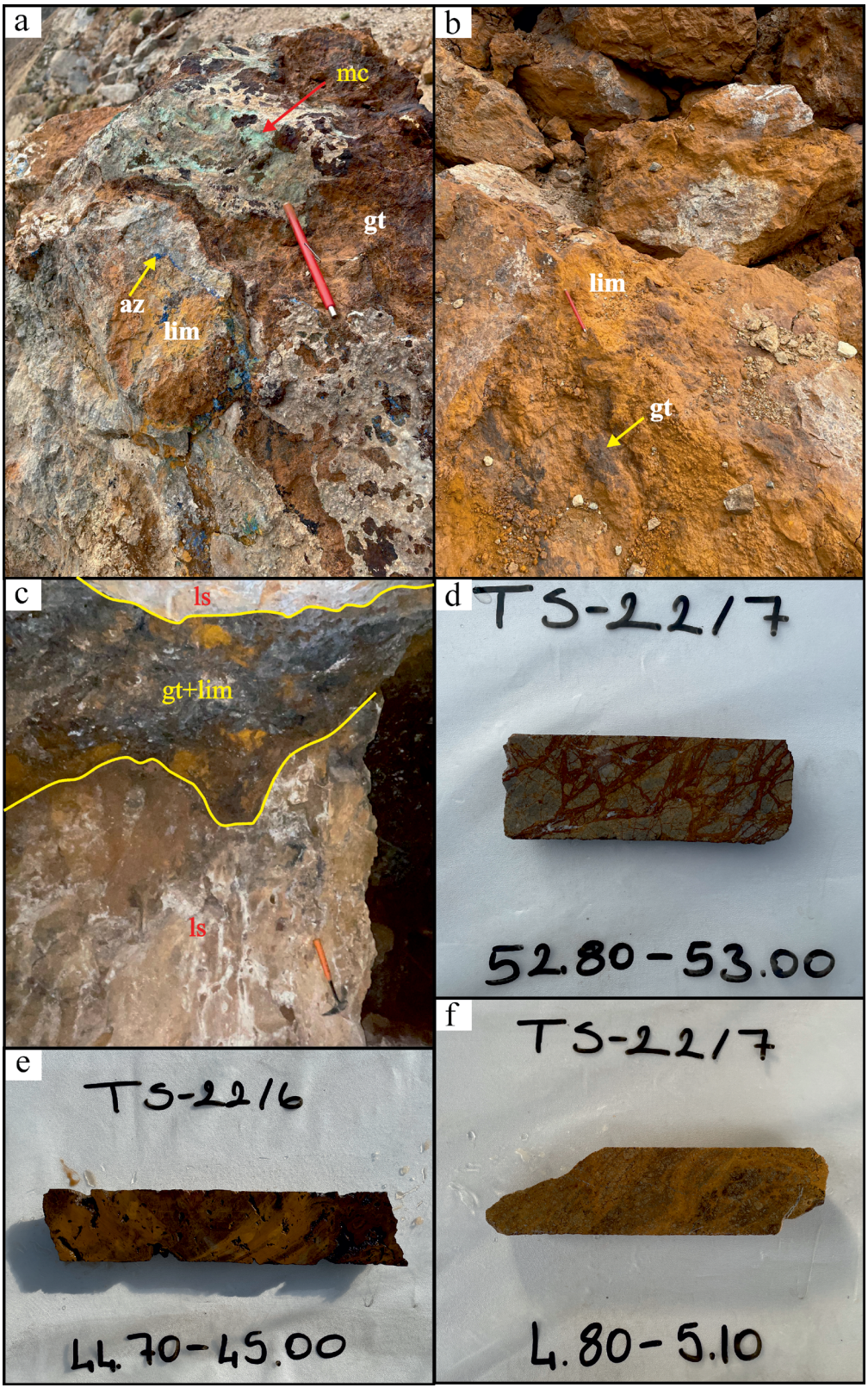

Figure 10- a) Field image of partially limonitized goethite ore with malachite and azurite, b) field image of predominantly limonitize goethite ore, c) field image of goethite and limonite ore filling fracture zones within karstic caves, d) drill core image of brecciated ore with goethite filling the voids, e) drill core image of goethite ore exhibiting a botryoidal texture, f) drill core image of ankerite ore (mc: malackite, az: azurite, lim: limonite, gt: goethite, ls: limestone).

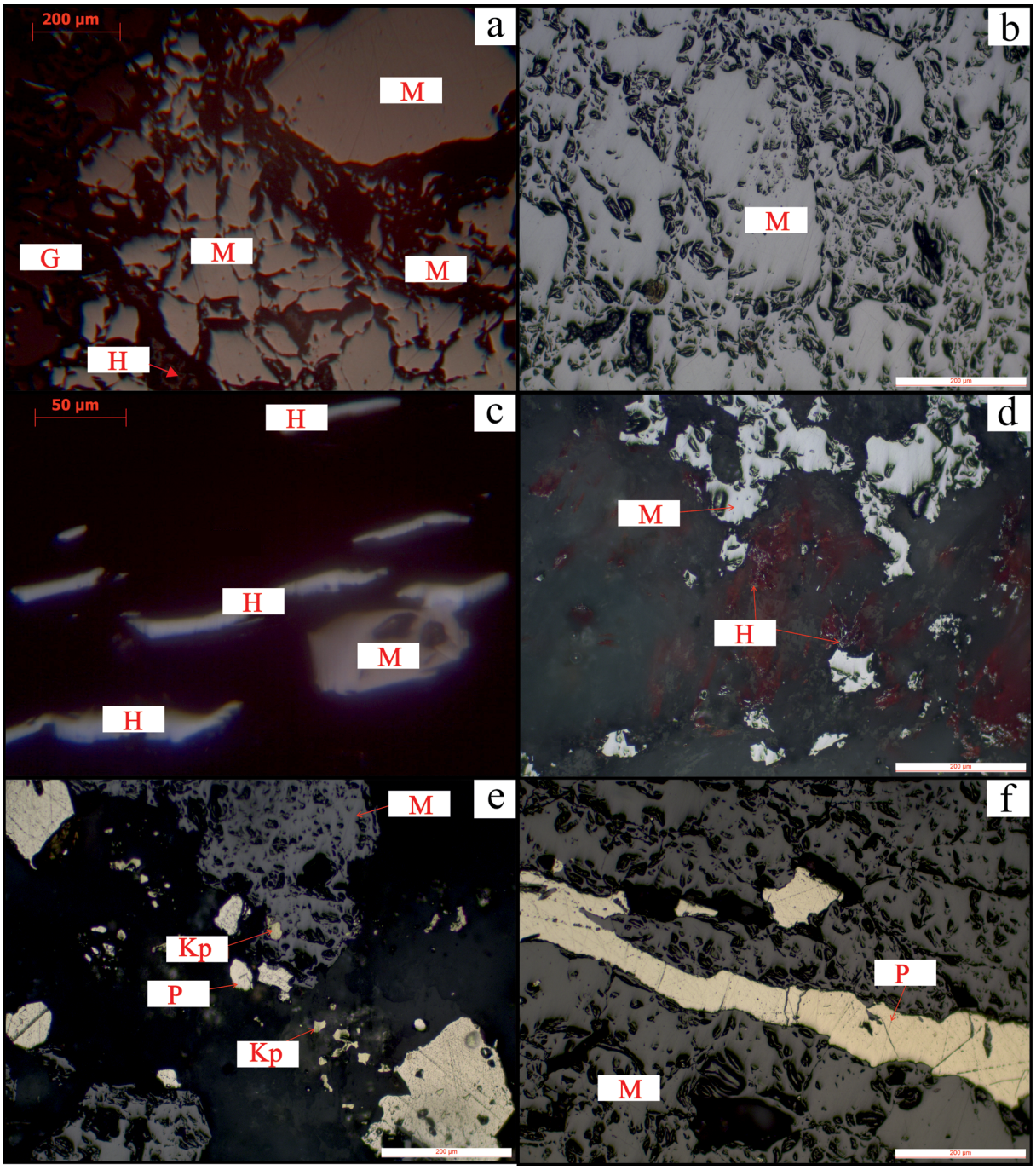

Figure 11- Microscope images of magnetite mineralization: a) angular and sub-angular magnetites of varying grain sizes, b) massive magnetites, c) oriented and hematitized magnetites, d) magnetites partially transformed into hematite due to martitization, e) pyrites and chalcopyrites of varying grain sizes within magnetites, f) pyrite vein cross-cutting the magnetites, (M: magnetite, H: hematite, P: pyrite, Kp: chalcopyrite, G: gangue mineral).

The results of these analyses are summarized in Table 1. According to this analysis: (1) Massive magnetite samples exhibit Fe_2O_3 contents ranging from 85.14% to 34.20%, with an average value of 56.91%. Ores with Fe_2O_3 contents below 50% can be readily upgraded to over 75% through magnetic separation. The SiO_2 contents in these samples vary significantly, with values as high as 41.40% and as low as 3.40%, averaging 19.67%. The increase in iron content during magnetic separation in facility

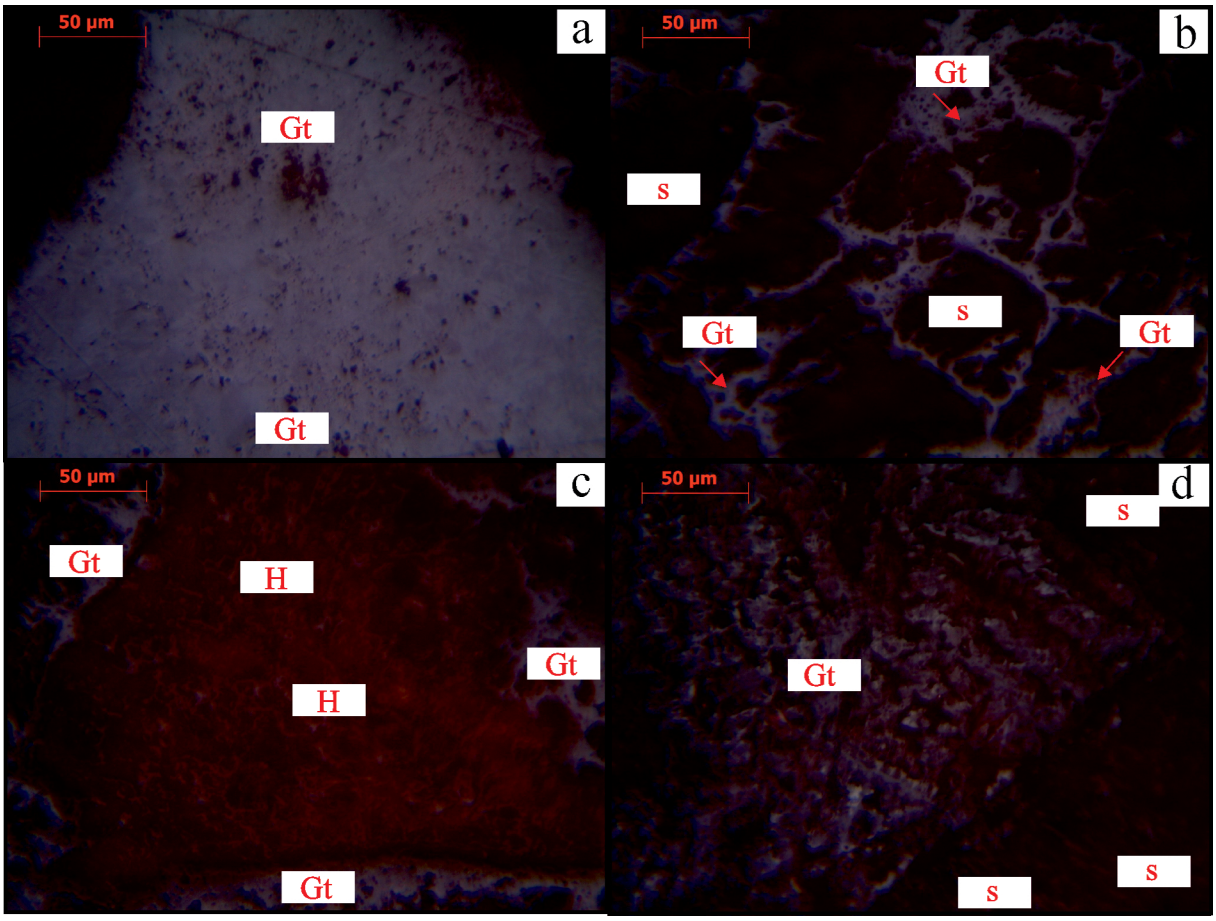

Figure 12- Microscope images of goethite-hematite mineralization: a) massive goethite, b) stockwork goethites with interstitial iron oxide coloring, c) remnant hematites among goethites, d) coarse-grained goethite with surrounding iron oxide coloring (Gt: goethite, H: hematite, s: iron oxide coloring).

suggests that SiO_2 is easily liberated and removed from the ore. (2) Disseminated magnetite samples display lower Fe_2O_3 contents, ranging from 38.20% to 7.26%. High-grade ores within this category can also undergo magnetic separation and be blended with massive ores for further processing and utilization. (3) Supergene-enriched ores located near the surface have Fe_2O_3 contents ranging from 75.90% to 38.60%. Geochemically, these ores share characteristics with the massive magnetites from which they originate. Due to their iron content and mineralogical properties, these supergene-enriched ores are suitable as raw materials for the cement industry. (4) Goethite samples exhibit Fe_2O_3 contents ranging between 85.60% and 7.46%, with an average of 61.65%. Among the analyzed samples, ankerites have the lowest iron content. While SiO_2 contents in goethite samples can reach up to 25.70%, the average SiO_2 value is 6.05%. Elevated SiO_2 contents are associated with the replaced outer zones containing lower iron content. High-iron content goethite samples are considered suitable for use in the steel industry due to their low impurity levels.

3. Discussion

3.1. Paragenesis and Succession

Based on the results, the paragenesis and succession of the Karadut Iron Mineralization suggest that the mineralization developed through five main stages (Figure 13). (i) The first stage represents the formation of magnetite mineralization. During this stage, magnetites formed in conformity with the host rocks, displaying laminated and stratified forms. These structures thin and thicken lens-like shapes, occasionally closing and reopening in lenticular

Table 1- Table of geochemical analysis results in Karadut iron mineralization ([1]massive ore, [2]disseminated ore, [3]martitized ore, [4]hydrothermal ore of goethite-hematite mineralization, my: magnetite, hem: hematite, gt: goethite, ank: ankerite).

Sample no	mineral type	mineralization type	Fe_2O_3 (%)	SiO_2 (%)	Al_2O_3 (%)	CaO (%)	K_2O (%)	MgO (%)	Na_2O (%)	TiO_2 (%)	LOI (%)
1	my	1	51.30	25.70	4.72	1.09	0.72	3.32	0.22	0.33	11.5
2	my	1	54.80	23.10	4.91	0.73	0.48	3.07	0.13	0.17	10.9
3	my	1	57.00	22.90	3.78	0.56	0.36	2.98	0.12	0.02	11.2
4	my	1	42.10	28.98	5.21	0.44	1.85	2.31	0.30	0.25	17.87
5	my	1	46.10	24.50	4.4	0.30	1.6	0.4	0.2	0.2	1.5
6	my	1	57.10	18.50	3.2	0.30	0.9	0.3	0.7	0.2	2.15
7	my	1	63.20	33.80	1.3	0.2	0.3	0.4	0.1	0.1	0.2
8	my	1	48.70	41.40	6.6	0.4	2.3	1.3	0.1	0.3	0.2
9	my	1	73.34	19.79	0.36	1.52	0.05	0.18	0.03	0.03	1.34
10	my	1	79.59	12.40	0.36	0.17	0.07	0.10	0.05	0.06	1.45
11	my	1	76.20	14.65	0.32	0.13	0.04	0.10	0.04	0.04	4.24
12	my	1	62.59	15.57	1.68	2.18	0.25	1.42	0.08	0.10	8.15
13	my	1	53.81	7.350	1.97	0.22	0.31	0.08	0.27	0.05	0.86
14	my	1	53.90	8.87	1.84	0.21	0.30	0.08	0.23	0.05	0.05
15	my	1	53.41	8.90	1.20	0.41	0.31	0.08	0.27	0.05	0.79
16	my	1	70.20	12.60	0.19	0.24	0.05	3.23	0.03	0.01	4.35
17	my	1	52.88	7.82	0.71	2.71	0.11	0.12	0.28	0.1	2.44
18	my	1	66.52	8.02	0.43	0.25	0.03	<0.01	0.08	0.05	<0.1
19	my	1	59.47	22.27	0.47	0.18	0.09	0.12	0.03	0.02	<0.1
20	my	1	67.91	8.92	0.26	0.15	0.03	0.05	0.10	0.06	4.01
21	my	1	34.20	32.40	4.5	1.5	0.7	19.0	0.2	0.2	6.5
22	my	1	40.00	13.70	0.09	20.1	0.04	1.61	0.13	0.05	23.60
23	my	1	40.20	17.80	0.36	8.93	0.14	2.19	0.15	0.02	29.90
24	my	1	66.70	6.80	0.8	0.2	0.1	0.2	0.2	0.1	2.40
25	my	1	47.75	23.25	0.6	0.1	0.2	0.4	0.05	0.05	16.80
26	my	1	47.00	22.08	2.46	0.37	0.084	0.12	0.11	0.13	0.41
27	my	1	44.00	38.90	2.17	0.63	0.16	1.03	0.16	0.6	9.94
28	my	1	41.50	25.70	0.47	2.08	0.1	0.23	0.19	0.1	11.50
29	my	1	53.30	3.40	1.31	20.31	0.083	1.34	0.11	0.044	18.33
30	my	1	59.50	34.20	1.1	3.1	0.3	0.6	0.1	<0.1	0.75
31	my	1	58.70	25.90	0.38	0.41	0.07	0.32	0.12	0.03	10.8
32	my	1	69.50	10.68	2.99	0.56	0.08	0.16	0.03	0.08	<0.1
33	my	1	73.80	8.92	2.54	0.58	0.03	0.13	0.08	0.07	<0.1
34	my	1	50.70	25.10	4.4	0.1	1.5	0.3	0.5	0.2	0.50
35	my	1	85.14	7.48	1.09	0.35	0.35	0.30	0.36	0.09	<0.1
36	my	1	60.48	16.30	2.46	0.24	1.02	0.24	0.34	0.13	<0.1
37	my	1	59.05	21.8	2.8	0.60	0.30	2.45	0.15	0.20	11.80
38	my	1	55.30	28.7	0.36	0.91	0.07	0.03	0.13	0.11	13.10
39	my	1	42.60	38.1	0.12	5.27	0.1	0.28	0.11	0.03	12.20
40	my	2	9.58	51.3	21.2	3.6	0.04	4.96	0.05	0.33	7.2
41	my	2	9.86	44.9	22.7	5.33	0.04	9.42	0.04	0.02	6.7
42	my	2	8.74	38.9	26.1	8.68	0.04	6.8	0.03	0.02	9.04
43	my	2	11.9	42.1	26.4	6.44	0.06	4.64	0.03	0.02	5.92
44	my	2	16.5	40.2	5.8	3.5	0.7	24.4	0.7	0.2	7.5
45	my	2	17.2	48.8	13.3	4.6	3.8	5.7	0.8	0.8	4.05
46	my	2	13.4	56.7	14.2	0.9	5.4	2.2	0.4	0.6	3.1
47	my	2	11.9	57.6	17.0	0.4	5.4	3.4	0.3	0.8	1.95
48	my	2	7.90	60.0	17.4	0.4	6.5	3.4	0.3	0.8	2.65
49	my	2	9.40	56.4	18.5	1.1	6.6	2.3	0.2	0.8	3.65
50	my	2	11.60	26.5	11.9	16.5	0.27	7.71	0.15	1.13	21.80
51	my	2	10.50	28.7	0.14	22.2	0.06	8.14	0.18	0.17	29.20

Table 1- continued.

Sample no	mineral type	mineralization type	Fe_2O_3 (%)	SiO_2 (%)	Al_2O_3 (%)	CaO (%)	K_2O (%)	MgO (%)	Na_2O (%)	TiO_2 (%)	LOI (%)
52	my	2	16.50	32.5	0.32	32.4	0.08	0.70	0.11	0.03	15.20
53	my	2	24.90	41.7	0.74	0.15	0.16	0.46	0.13	0.03	26.30
54	my	2	8.02	36.6	0.08	21.0	0.04	4.21	0.13	0.02	25.60
55	my	2	26.12	44.97	9.13	1.30	3.46	1.97	0.32	0.34	9.00
56	my	2	38.20	34.6	7.1	0.2	2.4	0.5	0.6	0.3	0.65
57	my	2	37.30	36.2	7.3	0.6	2.5	0.6	0.7	0.3	0.90
58	my	2	14.40	40.6	27.9	3.19	0.02	8.13	0.27	0.02	3.7
59	my	2	10.10	46	27.5	2.8	0.07	8.51	0.23	0.02	3.35
60	my	2	23.40	2.1	0.18	33.1	0.05	0.23	0.12	0.03	40.4
61	my	2	7.26	1.65	0.12	33.1	0.05	9.35	0.15	0.03	43.4
62	my	2	20.6	20.8	0.04	16.1	0.04	7.16	0.11	0.02	29.5
63	my	2	10.8	48.24	20.17	0.46	7.31	2.7	0.79	0.70	3.89
64	my	2	7.32	74.71	8.62	0.36	0.60	1.14	1.73	0.13	2.08
65	hem	3	52.3	1.5	1.51	18.2	0.07	0.5	0.19	0.07	23.4
66	hem	3	71.4	18.2	3.4	0.3	0.3	1.1	<0.1	0.1	4.45
67	hem	3	70.8	20.8	1.5	0.2	0.2	0.3	<0.1	0.2	5.40
68	hem	3	38.6	40.5	7.6	0.7	2.2	2.7	0.6	0.3	4.45
69	hem	3	45.87	19.23	0.78	1.09	0.44	1.42	0.06	0.17	8.34
70	hem	3	43.62	30.86	0.68	0.56	0.34	1.62	0.06	0.10	1.22
71	hem	3	75.9	14.5	0.6	0.4	0.3	0.7	<0.1	0.1	0.6
72	gt	4	65.5	4.28	2.87	3.85	0.14	0.39	0.13	0.12	14.5
73	gt	4	58.2	3.85	2.83	13.4	0.07	0.25	0.13	0.05	19.5
74	gt	4	71.3	2.1	1.13	6.72	0.05	0.22	0.15	0.02	15.9
75	gt	4	79.2	0.75	1.1	1.64	0.04	0.07	0.22	0.01	11.8
76	gt	4	76.9	2.99	1.32	2.94	0.06	0.27	0.24	0.02	13.8
77	ank	4	7.46	21.6	0.85	22.4	0.24	10.3	0.94	0.03	33.7
78	ank	4	8.12	25.7	0.19	16.8	0.04	11.1	0.05	0.02	25.7
79	hem	4	65.40	11.66	4.11	4.77	0.13	2.08	0.10	0.57	0.58
80	hem	4	65.20	12.44	2.48	0.41	0.12	0.14	0.14	0.09	0.82
81	hem	4	67.20	6.47	1.06	0.48	0.06	0.07	0.03	0.04	<0.1
82	hem	4	65.5	4.2	2.87	3.85	0.14	0.39	0.13	0.11	14.35
83	hem	4	52.3	1.36	1.40	18.27	0.07	0.48	0.17	0.03	23.57
84	hem	4	55.5	3.52	1.86	12.60	0.08	0.25	0.17	0.17	19.39
85	hem	4	71.3	2.08	1.13	6.65	0.041	0.21	0.15	0.02	15.84
86	hem	4	79.2	0.68	1.06	1.65	0.04	0.08	0.23	0.01	11.74
87	hem	4	76.9	2.92	1.22	2.98	0.05	0.26	0.25	0.02	13.96
88	ank	4	7.46	21.52	22.19	0.85	0.24	10.12	0.98	0.01	33.62
89	ank	4	14.4	17.8	0.19	25.9	0.02	8.13	0.27	0.02	31.60
90	ank	4	10.1	21.0	0.19	14.5	0.06	8.51	0.23	0.02	35.80
91	gt	4	80.2	1.3	10.75	4.1	<0.1	0.8	0.2	<0.1	0.1
92	gt	4	79.3	2.56	1.70	5.45	0.07	0.82	0.86	0.10	6.92
93	gt	4	85.5	1.86	1.43	1.21	0.04	0.76	0.63	0.14	4.21
94	gt	4	79.2	1.42	0.93	1.80	0.03	0.53	0.77	0.10	3.22
95	gt	4	83.6	0.95	0.46	0.65	0.04	0.81	0.85	0.17	5.32
96	gt	4	85.4	1.10	0.87	1.12	0.07	0.44	0.61	0.10	4.88
97	gt	4	85.3	0.97	1.32	2.86	0.05	0.63	0.85	0.14	3.95
98	gt	4	83.0	1.98	1.64	0.86	0.08	0.78	0.91	0.13	6.82
99	gt	4	85.6	0.81	0.73	1.92	0.06	0.56	0.75	0.12	3.65
100	gt	4	81.3	1.21	0.69	1.86	0.05	0.71	0.64	0.18	5.12
101	ank	4	24.0	0.50	0.10	39.00	<0.1	0.90	<0.1	<0.1	34.30

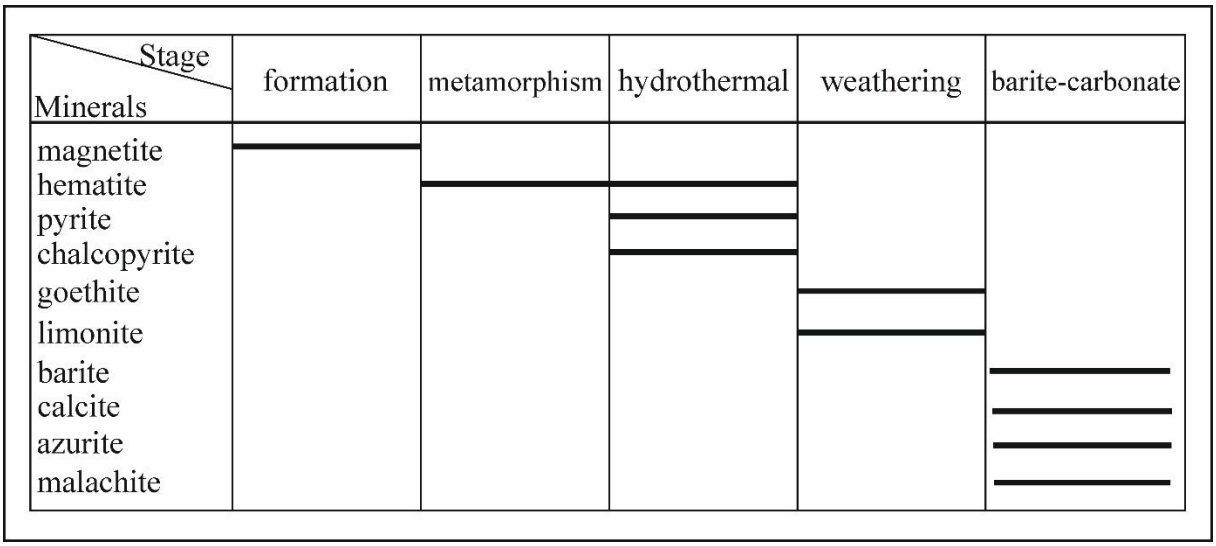

Figure 13- The paragenesis and succession diagram of Karadut Iron Mineralization formation.

patterns. (ii) In the second stage, partial martitization during metamorphism. This stage likely represents the transformation of magnetite into hematite due to metamorphic processes. These transformations are distinctly visible in polished sections. Hematite formations, aligned with the structural orientation observed in the field, are also attributed to this stage. (iii) The third stage is characterized by hydrothermal processes. Fluids influenced by the Havcılar Granite intrusion dissolved iron from the surrounding environment, forming iron-rich solutions. In oxygen-poor, low-pH acidic zones, iron precipitated as pyrite, whereas in oxygen-rich zones near the surface, particularly in karstic cavities and fracture zones, it precipitated as hematite. Pyrite veins crosscutting magnetites and chalcopyrite grains are linked to this stage. (iv) The fourth stage is the weathering phase. During this stage, hematites were largely transformed into goethites through weathering. Pyrites from the third stage, exposed to surface conditions via tectonic activity, underwent supergene alteration, resulting in the formation of limonite. (v) The fifth stage is the barite-carbonate and alteration phase. In this final stage, low-temperature fluids enriched with carbonate and barite precipitated among the stockwork goethites. Chalcopyrites were easily dissolved during this stage, forming malachite and azurite through interaction with carbonate-rich solutions.

4.2. Mineralisation Types

Iron mineralization classification relies on various factors, including the ore's structure and texture, its relationship with adjacent rocks, mineral paragenesis and succession, lithological and volcanic contexts, and age. This study summarizes the field and laboratory investigations conducted on the Karadut mineralization. To interpret the origin of the mineralization, more comprehensive studies, such as isotope analyses, are required. However, preliminary interpretations regarding the origin, along with literature data, have been synthesized with the findings of our research and presented below. In this way, it is aimed to convey our unverified hypotheses about the origin to the reader.

The magnetite mineralizations in the Karadut region were initially classified as itabirite-type sedimentary metamorphic mineralizations in preliminary studies conducted by the MTA (Atasever, 1978; Koç et al., 1985; Adıgüzel et al., 1991). However, "itabirite" is a term specific to Precambrian-aged, generally moderately to highly metamorphosed sedimentary iron deposits in Brazil. Globally, the term "banded iron formations (BIF)" is commonly used for layered and banded Precambrian-aged mineralizations. Although the Karadut mineralizations exhibit banded and metamorphic characteristics, their non-Precambrian age makes the terms "BIF" or "itabirite" inapplicable.

Gross (1970) introduced the term "layered iron deposits or iron formations" for banded, stratified, or laminated sediments containing 15% or more iron.

The texture and structure of the Karadut magnetite mineralization-banded, laminated, and lenticular forms, along with disseminated occurrences in the host rock-indicate a syngenetic origin. This interpretation is supported by microscopic observations. Given that the host schists were deposited in a marine environment, the mineralization can also be classified as marine sedimentary. According to Chukhrov (1974), iron can be transported as ferrobicarbonate on the surface in humid climates, with chemical weathering products subsequently transported to marine basins. These products are then deposited as oolitic hematite in coastal areas and as oolitic silicate or oolitic siderite in deeper marine zones, influenced by the CO_2 partial pressure. Elevated CO_2 concentrations lead to siderite precipitation rather than silicate (Oygür, 1991). Marine sedimentary iron deposits are typically dominated by oolitic structures (Bubenicek, 1961). The absence of oolites in the Karadut mineralization is likely due to post-depositional metamorphism. Consequently, the Karadut mineralization is best described as "metamorphic marine sedimentary type." Adıgüzel et al. (1991) suggested that the Karadut mineralization originally formed as hematite in a marine environment and was later enriched and transformed into magnetite through metamorphism and tectonic processes.

Goethite-hematite mineralizations, observed in massive and brecciated forms with barite, are hosted within karstic voids, fractures, and cracks in the wall rock. These characteristics are consistent with hydrothermal mineralization. Evidence supporting this includes the textural and structural properties of the ore, sharp contacts with the wall rock, and brecciated textures where hematite cements angular to subangular wall-rock fragments. The Havcılar Granite, intruded during the Early–Middle Eocene, is identified as the heat source that generated the hydrothermal solutions. Despite its iron-poor composition (based on literature and field observations), the Havcılar Granite likely mobilized iron from the "metamorphic marine sedimentary type" magnetites. Pyrite veins crosscutting magnetite mineralizations in thin sections further indicate a genetic relationship between hydrothermal and sedimentary mineralizations, supporting a post-Devonian formation age for the hydrothermal deposits.

Acknowledgements

This article was prepared by Şimşek Group Construction and Mining Company and is based on the data obtained during the exploration and exploitation activities conducted in the license area during 2021-2022. The authors extend their gratitude to the referees for their valuable criticisms and suggestions, which contributed significantly to the improvement of this article.

This article is dedicated to Prof. Dr. Taner Ünlü, who passed away approximately one year ago. Prof. Ünlü, the master's and doctoral advisor of the first author, was a distinguished scholar who devoted great effort to the exploration and development of Türkiye's iron deposits and became a pioneer in the field through numerous scientific publications. We bow respectfully to his memory.

References

Adıgüzel, O., Sarı, İ., Baysal, M. 1991. Kahramanmaraş-Elbistan-Çardak-Ericek-Berit Dağı Yöresi Demir Yatakları Maden Jeolojisi Raporu. Maden Tetkik Arama Genel Müdürlüğü, Rapor No: 9295, 51, Ankara (unpublished).

Atasever, İ. 1978. K. Maraş-Elbistan-Çardak-Mendikli-Havcılar Demir Zuhurları Jeoloji Raporu Maden Tetkik Arama Genel Müdürlüğü, Rapor No: 6804, 34, Ankara (unpublished).

Bahçeci, A. 1978. Hatay-Kırıkhan-Kastal Demir Madeni Jeoloji Ön Raporu. Maden Tetkik Arama Genel Müdürlüğü, Rapor No: 6693, 57, Ankara (unpublished).

Baydar, O. 1989. Berit-Kandil Dağları (Kahramanmaraş) ve Civarının Jeolojisi: İ.Ü. Fen Bilimleri Enstitüsü, PhD Thesis, 248, İstanbul, (unpublished).

Bedi, Y., Yusufoğlu, H. 2018. 1/100.000 Ölçekli Açınsama Nitelikli Türkiye Jeoloji Haritaları. Malatya–L40 paftası. No: 261., 94, Ankara.

Bedi, Y., Yusufoğlu, H., Usta, D., Okuyucu, C. 2012. The Presence of the Aladağ and Yahyalı Nappes in the Eastern Taurides (Afşin-Malatya) and their Tectonostratigraphic Characteristics: Paleozoic of

Northern Gondwana and Its Petroleum Potential. A Field Workshop Extended Abstracts, 09-14 th September 2012, Turkish Association Petroleum Geologists, Special Publication 6, 24-27, Kayseri.

Bedi, Y., Krystyn, L., Tekin, U.K., Okuyucu, C., Saydam-Demiray, D. G. 2016. Jeopark Alanı: Domuzdağ Napı'nda yer alan geç Karniyen yaşlı Ammonoid Toplulukları (Doğu Toroslar, Elbistan, Kahramanmaraş). 69. Türkiye Jeoloji Kurultayı Bildiri Özleri, 214-215, Ankara.

Bedi, Y., Şenel, M., Usta, D., Özkan, M. K., Beyazpirinç, M. 2004. Binboğa Dağları'nın Jeolojik Özellikleri ve Batı-Orta Toroslar'daki Benzer Birimler ile Deneştirilmesi. 57. Türkiye Jeoloji Kurultayı Bildiri Özleri, 271-272, Ankara.

Bedi, Y., Usta, D., Özkan, M. K., Beyazpirinç, M., Yıldız, H., Yusufoğlu, H. 2005. Doğu Toroslar'da (Göksun-Sarız-Elbistan) Allokton İstiflerin Tektono- Stratigrafik Özellikleri. 58.Türkiye Jeoloji Kurultayı Bildiri Özleri, 262-263, Ankara.

Bedi, Y., Yusufoğlu, H., Beyazpirinç, M., Özkan, M.K., Usta, D., Yıldız, H. 2009. Doğu Toroslar'ın Jeodinamik Evrimi (Afşin-Elbistan-Göksun-Sarız dolayı). Maden Tetkik Arama Genel Müdürlüğü, Rapor No: 11150, 388, Ankara (unpublished).

Bedi, Y., Yusufoğlu, H., Tekin, U. K., Usta, D. 2017*a*. Tufanbeyli (Adana), Elbistan (K.Maraş) ve Malatya Arasında Yüzeylenen Otokton ve Allokton İstiflerin Tektono-Stratigrafik Özellikleri. 70, Türkiye Jeoloji Kurultayı Bildiri Özleri, 22-23, Ankara (unpublished).

Bedi, Y., Yusufoğlu, H., Usta, D., Özkan, M. K., Beyazpirinç, M., Baran, C., Karakuş, E. 2017*b*. Doğu Toroslar'ın Jeodinamik Evrimi (Elbistan-Malatya-Elazığ). Maden Tetkik Arama Genel Müdürlüğü, Rapor No: 13731, V-I-II 1228, Ankara (unpublished).

Bubenicek, L. 1961. Recherces sur la Constituon et la Repartition du Minerai de fer dans 1' Aalenien de Lorraine. Science Terre 8, 5-204.

Bulur, K. 1969. Kahramanmaraş Bakır Sahalarının Prospeksiyonu ile İlgili Ön Rapor Teklifleri, Maden Tetkik Arama Genel Müdürlüğü, Rapor No: 12103, Ankara (unpublished).

Chukhrov, F.V. 1974. Evolution of Mineral Composition in Sedimentary Iron Ores. International Geology Review, 16, 161-168.

Cihnioğlu, M., İşbaşarır, O., Ceyhan, Ü., Adıgüzel, O. 1994. Türkiye Demir Envanteri. Maden Tetkik Arama Genel Müdürlüğü Envanter Serisi, 367, Ankara.

Çalgın, R., Şişman, N. 1974. MTA Enstitüsü'ne Ait 14/B No›lu Bakır-Kurşun-Çinko Sahası Prospeksiyon Raporu. Maden Tetkik Arama Genel Müdürlüğü, Rapor No: 5384, 13, Ankara (unpublished).

Göncüoğlu, M. C., Turhan, N. 1985. Bitlis Metamorfik Kuşağı Orta Bölümünün Temel Jeolojisi. Maden Tetkik Arama Genel Müdürlüğü, Rapor No: 7707, 216, Ankara (unpublished).

Gross, G. A. 1970. Nature and Occurrence of Iron Ore Deposits in Survey of World Iron Ore Resources. United Nations, 13-31, New York.

Karaman, T., Poyraz, N., Bakırhan, B., Alan, İ., Kadınkız, G., Yılmaz, H., Kılınç, F. 1993. Malatya-Doğanşehir-Çelikhan Dolayının Jeolojisi. Maden Tetkik Arama Genel Müdürlüğü, Rapor No: 9587, Ankara (unpublished).

Karaoğlan, F. 2012. Geochronology of the Ophiolitic and Granitic Rocks along the SE Anatolian Orogen. PhD Thesis. Çukurova University, Adana (in Turkish with English abstract).

Karaoğlan, F., Parlak, O., Klötzli, U., Koller, F., Rızaoğlu, T. 2013. Age and Duration of İntra-Oceanic Arc Volcanism Built on a Suprasubduction Zone Type Oceanic Crust in Southern Neotethys, SE Anatolia. Geoscience Frontiers 4, 399-408.

Kıral, N., Bedi, Y. 2019. Kahramanmaraş-Elbistan-Karadut Köyü Ar: 201700026 (Er:3345076) No'lu IV. Grup Feldispat Ruhsat Sahasına Ait Buluculuğa Esas Maden Jeolojisi ve Kaynak Kestirim Raporu. Maden Tetkik Arama Genel Müdürlüğü, Rapor No: 5714, 960, Ankara (unpublished).

Koç, İ., Kuşçu, A. E., Cengiz, R., Büyükgıdık, H., Aydoğan, M. 1985. Kahramanmaraş-Göksun-Elbistan-Çardak Yöresi Demir Prospeksiyonu Jeoloji Raporu. Maden Tetkik Arama Genel Müdürlüğü, Rapor No: 7910, 49, Ankara (unpublished).

Kraeff, A. 1964. Elbistan Bakır Ruhsat Sahası. Maden Tetkik Arama Genel Müdürlüğü, Rapor No: 3427, 7, Ankara (unpublished).

Metin, S., Ayhan, A., Papak, İ. 1986. Doğu Toroslar'ın Batı Kesiminin Jeolojisi (GGD Türkiye). Maden Tetkik ve Arama Dergisi, 107, 1-13.

Metin, S., Papak, İ., Keskin, H., Özsoy, İ., Polat, N., Altun, İ., İnanç, A., Haznedar, H., Konuk, O., Karabalık, N. N. 1982. Tufanbeyli-Sarız-Göksun ve Saimbeyli Arasının Jeolojisi (Doğu Toroslar). Maden Tetkik Arama Genel Müdürlüğü, Rapor No: 7129, Ankara (unpublished).

Nurlu, N., Parlak, O., Robertson, A. 2014. Güneydoğu Anadolu'da Ofiyolitik Kayaçları Kesen

Granitoyid İntrüzyonlarının Geç Kretase U-Pb Zirkon Yaşlarının Toros Allokton Topluluğu Açısından Olası Sonuçları (Kahramanmaraş Bölgesi). 67. Türkiye Jeoloji Kurultayı Bildiri Özleri, 54-57, Ankara (unpublished).

Oygür, V. 1991. Demir Cevherlerinin Değerlendirilmesinde Temel İlkeler. Jeoloji Mühendisleri Odası Yayınları No: 22, 102, Ankara.

Parlak, O. 2006. Geodynamic significance of granitoid magmatism in the southeast Anatolian orogen: geochemical and geochronogical evidence from Göksun-Afşin (Kahramanmaraş, Turkey) region. International Journal of Earth Sciences 95, 609-627.

Parlak, O., Rızaoğlu, T., Bağcı, U., Karaoğlan, F., Hoeck, V. 2009. Tectonic significance of the geochemistry and petrology of ophiolites in southeast Anatolia. Tectonophysics 473, 173–187.

Parlak, O., Karaoğlan, F., Klötzli, U., Koller, F., Rızaoğlu, T. 2010. Geochronology of ophiolites in Turkey: implications for Neotethyan geodynamics in eastern Mediterranean. 20th General Meeting of the International Mineralogical Association, 21-27 August 2010. Abstract Series. ACTA Mineralogica-Petrographica 6, 585.

Parlak, O., Karaoğlan, F., Rızaoğlu, T., Nurlu, N., Bağcı, U., Höck, V., Öztüfekçi Önal, A., Kürüm, S., Topak, Y., 2013. Petrology of the Ispendere (Malatya) ophiolite from the Southeast Anatolia: implications for the Late Mesozoic evolution of the southern Neotethyan Ocean. In: Robertson, A.H.F., Parlak, O. And Ünlügenç, U.C. (eds), Geological Development of Anatolia and the Easternmost Mediterranean Region. Geological Society, London, Special Publications, 372, 219-247.

Pehlivan, Ş., Barkurt, M.Y., Bilginer, E., Kurt, Z., Sütçü, Y.F., Can, B., Bilgi, C., Örçen, S., Süer, T., Karabıyıkoğlu, M. 1991. Elbistan-Nurhak (Kahramanmaraş) dolayının jeolojisi. Maden Tetkik ve Arama Genel Müdürlüğü Rapor No: 9423, Ankara (unpublished).

Perinçek, D. 1979. Geological Investigation of the Çelikhan-Sincik-Koçali Area (Adıyaman province). İstanbul Üniversitesi Fen Fakültesi Mecmuası 44, 127-147.

Perinçek, D. Kozlu, H. 1984*a*. Afşin-Elbistan-Doğanşehir Dolayının Stratigrafisi ve Bölgedeki Birliklerin Yapısal İlişkileri. Türkiye Petrolleri Anonim Ortaklığı Rapor No: 1909, Ankara (unpublished).

Perinçek, D., Kozlu, H. 1984*b*. Stratigraphy and Structural Relations of the Units in the Afşin-Elbistan-Doğanşehir Region (Eastern Taurus). In Tekeli, O. and Göncüoğlu, M.C (Eds), International Symposium on the Geology of the Taurus Belt, 181-198.

Polat, H. 1970. Maraş-Göksun İlçesi Bakır Sahasının Jeofizik Ön Etüdü. Maden Tetkik Arama Genel Müdürlüğü, Rapor No: 4581, Ankara (unpublished).

Robertson, A. H. F., Parlak, O., Ustaömer, T. 2012. Overview of the Palaeozoic-Neogene evolution of Neotethys in the Eastern Mediterranean region (S Turkey, Cyprus, Syria). Petroleum Geoscience 18, 381–404.

Robertson, A. H. F., Parlak, O., Ustaömer, T. 2013. Late Paleozoic-Early Cenozoic tectonic development of Southern Turkey and the Easternmost Mediterranean Region: Evidence from the İnner-Relations of Continental and Oceanic Units. Geological Society, Special Publications 372, 9-48, London.

Şenel, M., Bedi, Y., Metin. Y., Dalkılıç, H., Keskin, H., Kuru, K., Alan, İ., Balcı, V., Vergili, Ö., Usta, D., Usta, M., Tok, T., Şahin, Ş., Özkan, M. K., Taptık, M. A., Kop, A. 2002. Doğu Toroslar'ın batı kesiminin stratigrafik ve yapısal özellikleri, komşu bölgelerle korelasyonu. 55. Türkiye Jeoloji Kurultayı Bildiri Özleri, 249, Ankara.

Tarhan, N. 1982. Göksun-Afşin-Elbistan Dolayının Jeolojisi: Maden Tetkik Arama Genel Müdürlüğü, Rapor No: 7296, 63, Ankara (unpublished).

Tarhan, N. 1984. Göksun-Afşin-Elbistan Dolayının Jeolojisi. Jeoloji Mühendisliği Dergisi 19, 3-9.

Vergili, Ö., Taptık, M. A., Çetiner, L. 2017. Kahramanmaraş-Afşin-Hüyüklü (Kayışındere) (ER: 1094184) Porfiri Bakır-Molibden Sahası Buluculuk Talebine Esas Maden Jeolojisi ve Rezerv Raporu, Maden Tetkik Arama Genel Müdürlüğü, Rapor No: 13634, Ankara (unpublished).

Yazgan, E. 1981. Doğu Toroslar'da Etkin Bir Paleo-Kıta Kenarı Etüdü (Üst Kretase-Orta Eosen), Malatya-Elazığ, Doğu Anadolu. Yerbilimleri 7, 83-104.

Yazgan, E. 1984. Geodynamic Evolution of the Eastern Taurus Region. In Tekeli, O., Göncüoğlu, M.C. (Eds.). The International Symposium on Geology of the Taurus Belt, Maden Tetkik ve Arama Genel Müdürlüğü, Ankara, Turkey, 199-208.

Yıldırım, M. 1989. Kahramanmaraş Kuzeyindeki (Engizek-Nurhak Dağları) Tektonik Birliklerin Jeolojik-

Petrolojik İncelemesi, İstanbul Üniversitesi Fen Bilimleri Enstitüsü, PhD Thesis, 306, İstanbul, (unpublished).

Yılmaz, Y., Yiğitbaş, E., Yıldırım, M. 1987*a*. Güneydoğu Anadoluda Triyas Sonu Tektonizması ve Bunun Jeolojik Anlamı, Türkiye 7. Petrol Kongresi, 65-77.

Yılmaz, Y., Gürpınar, O., Kozlu, H., Gül. M. A., Yiğitbaş, E., Yıldırım, M., Genç, C., Keskin, M. 1987*b*. Maraş Kuzeyinin Jeolojisi (Andırın-Berit-Engizek-Nurhak-Binboğa Dağları) Yapı ve Jeolojik Evrimi, İstanbul Üniversitesi Mühendislik Fakültesi, 97, İstanbul.

Yılmaz, A., Bedi, Y., Yusufoğlu, H., Atabey, E, Aydın, N. 1997. 1/100.000 Ölçekli Açınsama Nitelikli Türkiye Jeoloji Haritası Serisi, Sivas-H23 Paftası, Maden Tetkik Arama Genel Müdürlüğü, 14, Ankara.

Yiğitbaş, E. 1989. Engizek Dağı (K.Maraş) Dolayındaki Tektonik Birliklerin Petrolojik İncelemesi, İstanbul Üniversitesi Fen Bilimleri Enstitüsü, PhD Thesis, 347, İstanbul (unpublished).

Zaralıoğlu, M., İnan, A. 1982. Kahramanmaraş-Afşin-Türksevin Köyü Dinarı Gediği Mevkisi Kurşun Cevherleşmesine Ait Jeoloji Raporu, Maden Tetkik Arama Genel Müdürlüğü, Rapor No: 7187, Ankara (unpublished).